Induced or triggered? The deadly February 2019 Rongxian-Weiyuan ML 4.9 earthquake in the shale gas field in Sichuan, China

Hongfeng Yang[1*], Pengcheng Zhou [1], Nan Fang[2] , Gaohua Zhu [1], Wenbin Xu[2], Jinrong Su[3], Fanbao Meng[1], and Risheng Chu[4]

[1]Earth System Science Programme, Faculty of Science, The Chinese University of Hong Kong, Sha Tin, Hong Kong, China (hyang@cuhk.edu.hk)
[2]School of Geoscience and Info-physics, Central South University, Changsha, China
[3]Earthquake Monitoring Centre, Sichuan Earthquake Administration, Chengdu, China
[4]Institute of Geodesy and Geophysics, Chinese Academy of Sciences, Wuhan, China

➢ 1. Introduction

Felt earthquakes become a major concern near hydraulic fracturing (HF) sites in the Southern Sichuan Basin (SSB), China [Lei et al., 2019; Meng et al., 2019].

❖ Motivations

On 25 February 2019, a magnitude M_L 4.9 earthquake (hereafter mainshock) struck the Rongxian County, preceded ~8h by a M_L 4.3 earthquake and ~32h by a M_L 4.7 earthquake. Reported with 2 fatalities and 12 injuries, they raised great concerns and large societal impacts. What are the responsible faults of the deadly earthquakes and the potential link with HF were critical not only for seismic hazard assessment in the region, but also for secure and continuous development of shale gas industry in China.

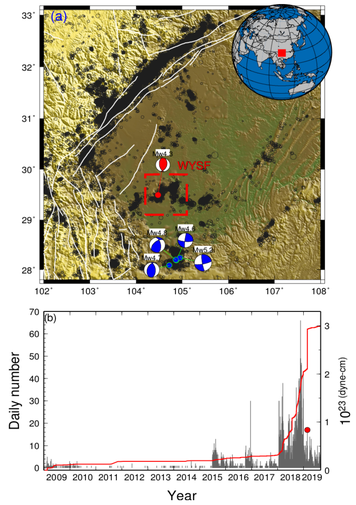

Figure 1. Surging earthquakes in the Sichuan Basin.
(a) Seismicity with local magnitudes larger than 1 since December 2008 are shown by black circles. White lines represent mapped faults. Blue beach balls denote moment tensor solutions of induced earthquakes in the Changning region [*Lei et al.*, 2019]. Red beach ball indicates the 25 February 2019 M_w 4.3 (M_L 4.9) earthquake. WYSF: Weiyuan Shale Gas Field **(b)** Daily number of earthquakes (M_L>1) in the Rongxian-Weiyuan region with location shown in (a) by the red dashed lines. Red line denotes seismic moment release from December 2008 to March 2019. Red dot marks the occurrence time of the 25 February 2019 mainshock.

➢ 2. Data

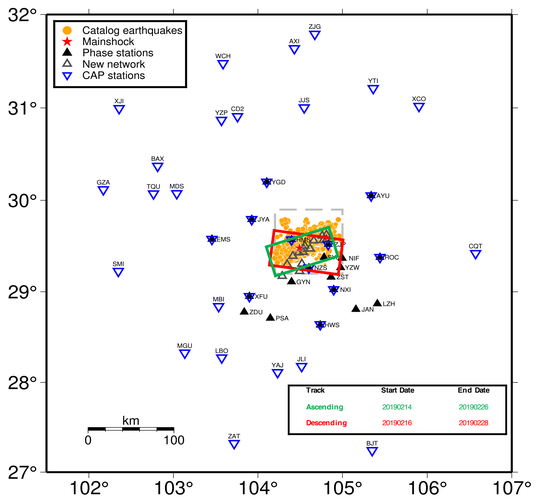

Figure 2. Seismic data and Sentinel-1 satellite data.
Catalog earthquakes from September 1, 2018 to March 13th 2019 (yellow dots) and seismic stations used in this study. Black triangles denote stations that were used for relocations. Blue stations are used in focal mechanism determination. Grey triangles denote stations that were deployed after the mainshock (red star). Grey dashed lines bound the area shown in Fig. 3a.

➢ 3. Earthquake relocations and focal mechanisms

- ❖ The relocated earthquakes are separated in two clusters and the Rongxian-Weiyuan cluster correlates with the Molin fault.
- ❖ Aftershocks, mostly < 5 km, are located on both sides of the Molin fault (a west-dipping reverse fault).
- ❖ We use Cut and Paste (CAP) method [Zhu & Helmberger, 1996] to invert focal mechanisms of M_L 4 earthquakes, using broadband seismic stations within 300 km.

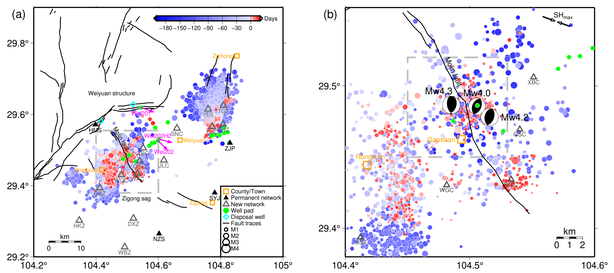

Figure 3. Relocated earthquakes and focal mechanisms.
(a) Mapped faults (black lines), local seismic stations (black and grey triangles), and relocated earthquakes (color dots) with colors showing their occurrence time relative to the origin time of the mainshock. Green diamonds denote locations of hydraulic fracturing wells. Purple arrows show directions of maximum horizontal stress from borehole measurements. Dashed grey lines denote the area shown in **(b),** a zoom-in map showing earthquake locations and moment tensor solutions of the three M4+ earthquakes.

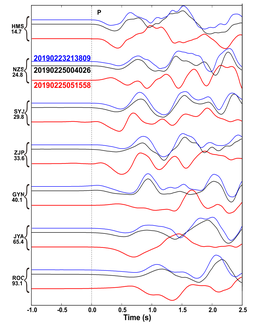

Figure 4. Waveform comparison.
The mainshock (red) and the two M4 foreshocks (blue and black) at station across different distances, shown on left. All waveforms were aligned by our manually picked P wave arrivals.

➢ 4. Rupture dimensions

- ❖ We explore the parameter space of a rectangular dislocation source [Okada, 1985] and conduct uncertainty estimations with a Beyesian method [Tarantola, 2005].
- ❖ **West-dipping reverse fault** (length/width, 4.37km/0.4km).

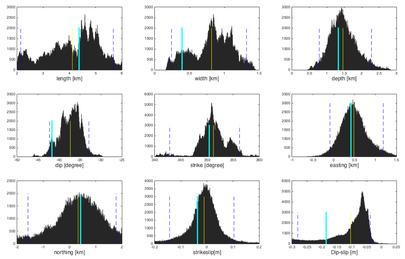

Figure 5. Posterior probability distribution for the parameters of the Rongxian earthquake model.
The yellow line shows the mean value of the parameters. The cyan line shows the maximum posteriori value of the parameters. The blue dashed lines show the 95% confidence intervals for each parameter.

➢ 5. Seismicity and fault geometry

- ❖ The fault geometry of the mainshock derived from seismic data agrees with InSAR results.
- ❖ Fluid migration into the Molin fault is unlikely, as there is a 800-m thick shale layer atop the formation where fracking was conducted.

Table 1. Depth comparison.

Events	Hydraulic fracking	M4 foreshocks	Mainshock	Aftershocks
Depth(km)	~ 2.7	2.6, 2.7	1	Mostly, 2 to 6

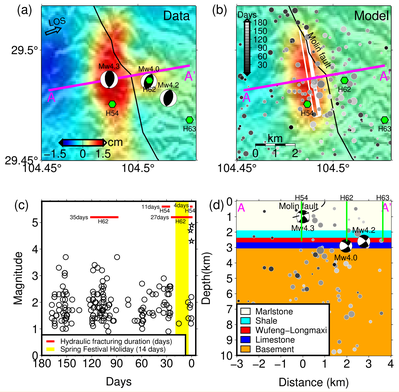

Figure 6. InSAR data and the mainshock deformation model.
(a) Observed ground deformation (color) and moment tensor solutions from seismic data. Black line is the Molin fault. Green hexagons denote fracking wells. **(b)** Best-fit source model from InSAR data and seismicity (grey dots) in 180 days before the mainshock. AA' denotes a cross sections shown in (d). **(c)** Local magnitude of seismicity (circles) before the three M4+ earthquakes (stars). Yellow stripe denotes the holidays after the Spring Festival. **(d)** Seismicity, moment tensor solutions, Molin fault, and fracking wells projected on the cross section of AA'. Background color denotes the simplified geological section.

➢ 6. Coulomb failure stress

- ❖ We calculate the static Coulomb failure stress changes (ΔCFS) caused by the two foreshocks on the mainshock's fault plane.
- ❖ Coulomb failure stresses of the two foreshocks on the Molin fault was ~0.03 bar, smaller than typical static triggering threshold (0.1 bar).

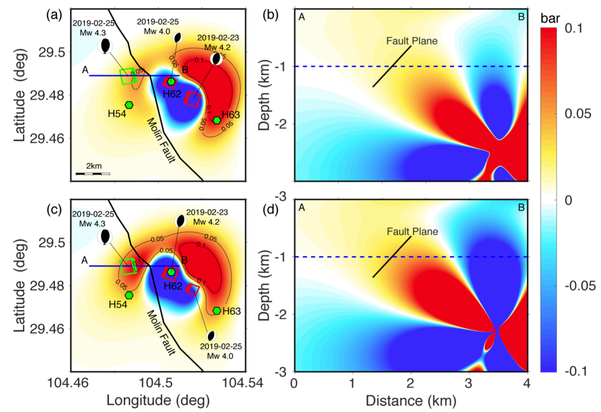

Figure 7. Coulomb failure stress (CFS) caused by the two foreshocks.
(a) map view of the Coulomb failure stress (color) caused by the two foreshocks (red rectangles) on the mainshock fault (green rectangle). Contour lines denote 0.05 and 0.1 bar, respectively. Nearby fracking well locations are shown by green hexagons. **(b)** CFS in the cross section whose location is shown in **(a)**. **(c)** and **(d)** are same to **(a)** and **(b)**, respectively, except for exchanging the locations of the two foreshocks.

➢ 7. Discussion

- ❖ Most of these earthquakes occurred at 2-6 km in depth, with the two M4 foreshocks at ~2.7 km, coinciding with the depth where fracking was conducted.
- ❖ The shallow depths contribute to strong shakings of the M_w 4 earthquakes and resulted damages.
- ❖ The mainshock was caused by the reactivation of the Molin fault, but the M_w 4 foreshocks likely occurred on an unmapped conjugate fault.
- ❖ We suggested that the deadly Rongxian-Weiyuan earthquake was plausibly induced by hydraulic fracturing through poroelastic stress transfer onto the Molin fault that was supposed to be aseismic at the shallow depth.

➢ References

Lei, X., Wang, Z., & Su, J. (2019). The December 2018 ML 5.7 and January 2019 ML 5.3 Earthquakes in South Sichuan Basin Induced by Shale Gas Hydraulic Fracturing. *Seismological Research Letters*, 90(3),1099-1110.

Meng, L., McGarr, A., Zhou, L., & Zang, Y. (2019). An Investigation of Seismicity Induced by Hydraulic Fracturing in the Sichuan Basin of China Based on Data from a Temporary Seismic Network. *Bull. Seismol. Soc. Am.*, 109 (1), 348-357.

Okada, Y. (1985), Surface deformation due to shear and tensile faults in a half-space, *Bull. Seismol. Soc. Am.*, 75, 1135–1154.

Tarantola, A. (2005). Inverse Problem Theory and Methods for Model Parameter Estimation, Society for Industrial and Applied Mathematics, Philadelphia, Pennsylvania.

Waldhauser, F., & Ellsworth, W. L. (2000). A double-difference earthquake location algorithm: Method and application to the Northern Hayward Fault, California. *Bull. Seismol. Soc. Am.*, 90(6), 1353–1368.

Zhu, L., & Rivera, L. A. (2002). A note on the dynamic and static displacements from a point source in multilayered media. *Geophysical Journal International*, 148(3), 619–627.